2013 IEEE/RSJ International Conference on
Intelligent Robots and Systems (IROS)
November 3-7, 2013. Tokyo, Japan

Hierarchical Underwater Localization in Dominating Background Flow Fields

Zhuoyuan Song, *Student Member, IEEE*, and Kamran Mohseni, *Member, IEEE*

***Abstract*— The effect of ocean flow on the motion of autonomous underwater vehicles (AUV) is often crucial in the development of underwater localization algorithms and should not be treated as small disturbances. The domination of strong ocean currents and the requirement of low power consumption prohibit AUVs to move against a background flow to obtain localization correction in a timely manner. Our recent studies, among others, enable an unmanned vehicle to follow a near optimal trajectory found by Lagrangian coherent structures based fluid control algorithm with minimal fuel usage, which improves the vehicles' runtime and the path following accuracy in the presence of strong background flow. Here, we propose a three-dimensional fully distributed localization hierarchy to improve the localization of low-cost mobile marine data collection underwater sensor networks using intra-vehicle communication and measurements. The proposed algorithm is realized by using the extended Kalman filter. Correlation terms in covariance matrices are considered independently to meet the distributed feature. Resulting simulated localization errors are bounded at satisfactory levels and the relationship between the number of AUVs and the performance of the algorithm is investigated.**

I. INTRODUCTION

In the formation of tropical storms and hurricanes, the air pressure, air humidity, air or water temperature and water salinity change drastically. The gradient distribution of these factors through air, ocean surface and undersea areas will help us to obtain a better understanding and forecast of them. The implementation of autonomous underwater vehicles (AUV) has shown increasing success and promise in meeting specific marine data collection requirements. However, the localization accuracy of these AUVs directly determines the quality of the collected data.

Underwater localization is a challenging topic since AUVs can rarely take advantage of the global position system (GPS) due to the rapid attenuation of radio frequency (RF) signals in water. Much related works have been done during the past decades [1], [2], [3], [4]. However, to the best of our knowledge, the effect of ocean flow has not been well accounted for in the development of underwater localization methods. In applications like marine data collection, impacts of background flow on AUVs cannot be considered as small disturbances. In most cases, small AUVs are not capable of moving against flow to approach localization references and to correct localization errors on time. Lipinski and Mohseni [5] have developed a ridge tracking algorithm for the computation and extraction of Lagrangian coherent structures (LSC). The proposed algorithm tracks ridges of the finite time Lyapunov exponent (FTLE) field at each time step and then approximates locations of ridges at the next time step by advecting the LCS forward with the flow. Relationships between optimal trajectories and coherent structures in background flow have been studied in several works [6], [7]. A procedure for trajectory planning based on LCS is outlined in [8]. In the presence of strong background flow, the proposed hybrid approach yields near fuel optimal trajectories given a cost function that combines fuel and time costs. These works enable AUVs navigating in strong background flow with moderate fuel usage. LCS based trajectories enable AUVs move as drifters and avoid moving against strong flow for the most of run-time, which ensures both navigation accuracy and endurance. Using these AUVs as moving references, we propose a three-dimensional fully distributed cooperative localization method to help the localization of other low-cost marine data collection AUVs. This work provides the essence of the proposed algorithm, describes the development of resultant covariance matrices and lays a foundation of further studies on cooperative data collecting systems of unmanned aerial vehicles (UAV) and AUVs.

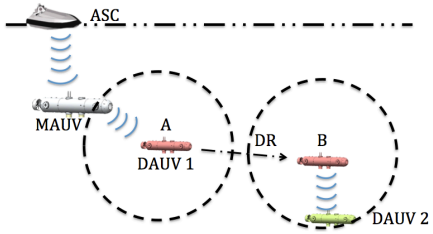

Fig. 1. Intra-vehicle cooperation illustration. The DAUV uses better-localized MAUVs as references to correct the location estimate at location *A* and performs dead reckoning (DR) during the translation from location *A* to location *B*, where it takes relative measurements and gets localization information from other DAUVs in the neighborhood if any of them has better localization estimates.

II. PROBLEM STATEMENT

AUVs can be divided into two groups, *i.e.* mother AUVs (MAUVs) and daughter AUVs (DAUVs) (Fig. 1). We assume that all AUVs have the two-way communication ability with others in the communication range. MAUVs are equipped with the standard AUV sensor suite, including inertial measurement units (IMU), magnetometers and Doppler velocity logs (DVL). Due to their relatively valuable equipment, the number of MAUVs is small. Autonomous surface crafts (ASCs) have access to the GPS, which helps MAUVs to sustain a relatively more accurate localization estimate by

Zhuoyuan Song is with Graduate Student in Dept. of Mech. and Aerosp. Eng. and Inst. of Networked Autonomous Syts., Univ. of Florida, Gainesville, Florida 32611, USA nick.songzy@ufl.edu

Kamran Mohseni is with William P. Bushnell Endowed Chair in Dept. of Mech. and Aerosp. Eng. and Dept. of Elect. and Comput. Eng., and with the Inst. of Networked Autonomous Syst., Univ. of Florida, Gainesville, Florida 32611, USA mohseni@ufl.edu

$$\mathrm{P}(D_{i,k},\mathcal{D}_{-i,k},\mathcal{M}_k|\mathcal{Z}^k,\mathcal{U}^k) = \eta \cdot \underbrace{\mathrm{P}(z_k^{\mathcal{D}}|D_{i,k},\mathcal{D}_{-i,k})}_{\text{CL Update}} \underbrace{\int \mathrm{P}(\mathcal{D}_{-i,k}|\mathcal{D}_{-i,k-1})\,\mathrm{P}(\mathcal{D}_{-i,k-1}|\mathcal{Z}^{\mathcal{D},k-1},\mathcal{U}^{k-1})\,d\mathcal{D}_{-i,k-1}}_{\text{CL Prediction}}$$

$$\underbrace{\mathrm{P}(z_k^{\mathcal{M}}|D_{i,k},\mathcal{M}_k)}_{\text{DSLAM Update}} \underbrace{\iint \mathrm{P}(D_{i,k}|u_k,D_{i,k-1})\,\mathrm{P}(\mathcal{M}_k|\mathcal{M}_{k-1})\,\mathrm{P}(D_{i,k-1},\mathcal{M}_{k-1}|\mathcal{Z}^{\mathcal{M},k-1},\mathcal{U}^{k-1})\,d\mathcal{M}_{k-1}\,dD_{i,k-1}}_{\text{DSLAM Prediction}}. \quad (1)$$

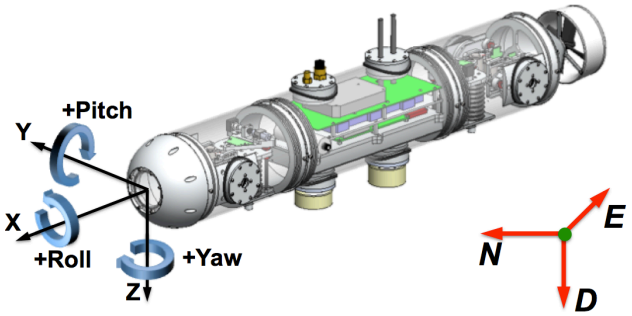

Fig. 2. Our fifth generation AUV "CephaloBot" [13], [14], [15], [16].

combining dead reckoning (DR) with moving long baseline (MLBL) [9], [10]. Based on coarse knowledge of the background flow, all MAUVs navigate along periodic near optimal paths generated by algorithms developed in [7] and [8]. The number of DAUVs is large and they are used specifically to collect marine data of interests. Assume all DAUVs are equipped with low-cost IMUs, scope-limited range and bearing sensors, and underwater communication units, along with data collection sensors. They are not capable enough to perform MLBL or high accuracy DR.

To mathematically represent the problem in the probability theory, we denote the collection of MAUVs' locations at time k as $\mathcal{M}_k$, where $\mathcal{M}_k = \{M_{1,k}, M_{2,k}, \ldots, M_{m,k}\}$ and m is the total number of MAUVs. For DAUV i, whose state at time k is denoted as $D_{i,k}$, the collection of positions of all other DAUVs at time k is $\mathcal{D}_{-i,k} = \{D_{n,k} \,|\, n = 1, 2, \cdots, d \cap n \neq i\}$ and d is the total number of DAUVs. The state of DAUV i, $D_{i,k}$, can be inferred using a probabilistic function given the previous position $D_{i,k-1}$ and the control input u_k, which could be an IMU measurement from time $k-1$ to time k. A relative distance measurement at time k is denoted as z_k. For simplicity, we have following collection definitions: $\mathcal{U}^k = \{u_0, u_1, \ldots, u_k\} = \{\mathcal{U}^{k-1}, u_k\}$ and $\mathcal{Z}^k = \{z_0, z_1, \ldots, z_k\} = \{\mathcal{Z}^{k-1}, z_k\}$.

In the probability theory, the joint posterior of all AUVs' locations, given all measurements and control inputs, is $p(D_{i,k},\mathcal{D}_{-i,k},\mathcal{M}_k|\mathcal{Z}^k,\mathcal{U}^k)$ when initial locations of all AUVs are known. This work does not depend on any static physical map features or landmarks. Instead, MAUVs are considered as dynamic landmarks, which turns the MAUV-aided localization correction problem into a dynamic simultaneous localization and mapping (DSLAM) problem. The multi-DAUV cooperation is a standard cooperative localization (CL) process. Related works have been done by Martinelli *et al.* [11] and Roumeliotis and Bekey [12]. Both works indicate the necessity of having at lease one vehicle with the global localization ability to bound the overall error.

Inspired by the decomposition method used by Wang *et al.* [17], a dynamic Bayes filter with Markov property for the formulated problem is developed. Assume that measurements at different time steps are mutually independent such that we can group them as $z_k = z_k^{\mathcal{D}} + z_k^{\mathcal{M}}$, where $z_k^{\mathcal{D}}$ are measurements among DAUVs and $z_k^{\mathcal{M}}$ are measurements between DAUVs and MAUVs. Hence, for a collection of measurements till time k, $\mathcal{Z}^k = \mathcal{Z}^{\mathcal{D},k} + \mathcal{Z}^{\mathcal{M},k}$. Dividing measurements in the joint posterior and performing necessary mathematical manipulations based on Markov property yield

$$\begin{aligned}\mathrm{P}(D_{i,k},\mathcal{D}_{-i,k},\mathcal{M}_k|\mathcal{Z}^k,\mathcal{U}^k) &\propto \underbrace{\mathrm{P}(z_k^{\mathcal{M}}|D_{i,k},\mathcal{M}_k)\,\mathrm{P}(D_{i,k},\mathcal{M}_k|\mathcal{Z}^{\mathcal{M},k-1},\mathcal{U}^k)}_{\text{Dynamic SLAM}} \\ &\times \underbrace{\mathrm{P}(z_k^{\mathcal{D}}|D_{i,k},\mathcal{D}_{-i,k})\,\mathrm{P}(\mathcal{D}_{-i,k}|\mathcal{Z}^{\mathcal{D},k-1},\mathcal{U}^k)}_{\text{Cooperative Localization}}. \end{aligned} \quad (2)$$

The posterior updating process has been factorized into DSLAM and CL. By using the theorem of total probability, (1) is the result of further factorizing (2) to introduce the updating process. The joint posterior is divided into two separated posteriors, $\mathrm{P}(\mathcal{D}_{-i,k-1}|\mathcal{Z}^{\mathcal{D},k-1},\mathcal{U}^{k-1})$ for CL, and $\mathrm{P}(D_{i,k-1},\mathcal{M}_{k-1}|\mathcal{Z}^{\mathcal{M},k-1},\mathcal{U}^{k-1})$ for DSLAM. This indicates that the recursive updating process for these two posteriors can be performed separately without interferences, which is crucial in a fully distributed algorithm.

III. Realization in the Extended Kalman Filter

A. Motion model

1) Single vehicle motion model: Unlike most ground SLAM applications, AUVs are modeled in 3D with six DOFs. Proprioceptive sensors (IMUs) provide changes in positions and orientations in a real-time manner. Since DR is an error accumulation process, at least one exterior reference must be provided to bound the drift in long distance movements. The IMU provides three-axis Euler angles or quaternions, it is more convenient to directly use yaw/pitch/roll angles in Tait-Bryan conventions. Assume the vehicle's initial position is chosen as the origin of the North/East/Down (NED) earth fixed coordinate system, denoted as G, and current Euler angles in this system are (ϕ, θ, ψ) (Fig. 2). Denote the local coordinate system attached to the vehicle as A and let the orientation of A be the result of rotating the coordinate system, initially aligned with the NED coordinate, around x axis by angle ψ, followed by a rotation along the resultant y axis by angle θ, and again along the resultant z axis by angle ϕ. Then the rotation matrix can be written as

$${}^{G}_{A}\boldsymbol{\mathcal{R}} = \begin{bmatrix} \mathrm{c}\phi\mathrm{c}\theta & \mathrm{c}\phi\mathrm{s}\theta\mathrm{s}\psi - \mathrm{s}\phi\mathrm{c}\psi & \mathrm{c}\phi\mathrm{s}\theta\mathrm{c}\psi + \mathrm{s}\phi\mathrm{s}\psi \\ \mathrm{s}\phi\mathrm{c}\theta & \mathrm{s}\phi\mathrm{s}\theta\mathrm{s}\psi + \mathrm{c}\phi\mathrm{c}\psi & \mathrm{s}\phi\mathrm{s}\theta\mathrm{c}\psi - \mathrm{c}\phi\mathrm{s}\psi \\ -\mathrm{s}\theta & \mathrm{c}\theta\mathrm{s}\psi & \mathrm{c}\theta\mathrm{c}\psi \end{bmatrix},$$

where $\mathrm{s}\phi = \sin(\phi)$ and $\mathrm{c}\phi = \cos(\phi)$. Intuitively, given the rotation matrix from frame G to frame A, ${}^{G}_{A}\boldsymbol{\mathcal{R}}$, and

the rotation matrix from frame A to frame B, ${}^A_B\boldsymbol{\mathcal{R}}$, the rotation matrix from frame G to frame B can be computed through ${}^G_B\boldsymbol{\mathcal{R}} = {}^G_A\boldsymbol{\mathcal{R}} \times {}^A_B\boldsymbol{\mathcal{R}}$. In the Euclidian space, the six-DOF state vector of the vehicle at time k can be expressed as $\mathbf{x}_k = [\ \mathbf{p}_k^T \quad \mathbf{o}_k^T\ ]^T = [\ x_k \quad y_k \quad z_k \quad \phi_k \quad \theta_k \quad \psi_k\ ]^T$, where $\mathbf{p}_k = [\ x_k \quad y_k \quad z_k\ ]^T$ is the position and $\mathbf{o}_k = [\ \phi_k \quad \theta_k \quad \psi_k\ ]^T$ is the orientation in Euler angles.

In original 2D SLAM problems and most other mobile robots applications, odometry or inertia sensor measurements are often used as control inputs to vehicles' dynamic models. Since three-dimensional rotations cannot be intuitively expressed in terms of increases in Euler angles and the IMU can directly provide Euler angles relative to the NED coordinate system, we use Euler angle measurements as orientation control inputs and the double integration of three-axis accelerations as position control inputs. The control driving the vehicle from $\mathbf{x}_k$ to $\mathbf{x}_{k+1}$ is $\boldsymbol{\tau}_{k+1} = [\ \delta x_{k+1} \quad \delta y_{k+1} \quad \delta z_{k+1} \quad \phi_{k+1} \quad \theta_{k+1} \quad \psi_{k+1}\ ]^T$, which is assumed to be corrupted by white Gaussian noises. Given aforementioned definitions, the motion model is

$$\mathbf{x}_{k+1} = \mathbf{f}\left(\mathbf{x}_k, \boldsymbol{\tau}_{k+1}, \boldsymbol{\epsilon}_{k+1}\right), \tag{3}$$

where $\boldsymbol{\epsilon}$ are control noises and the noise-free single vehicle motion model is

$$\begin{aligned}\mathbf{x}^-_{k+1} &= \mathbf{f}\left(\mathbf{x}_k, \boldsymbol{\tau}_{k+1}, \mathbf{0}\right)\\ &= \mathbf{I}_\alpha\ \boldsymbol{\tau}_{k+1} + \mathbf{I}_\beta\ \left(\ \mathbf{I}_\gamma\ \mathbf{x}_k + {}^G_{k+1}\boldsymbol{\mathcal{R}}\ \mathbf{I}_\gamma\ \boldsymbol{\tau}_{k+1}\delta t\ \right),\end{aligned} \tag{4}$$

$$\mathbf{I}_\alpha = \begin{bmatrix}\mathbf{0}_{3\times3} & \mathbf{0}_{3\times3}\\ \mathbf{0}_{3\times3} & \mathbf{I}_{3\times3}\end{bmatrix},\ \mathbf{I}_\beta = \begin{bmatrix}\mathbf{I}_{3\times3} & \mathbf{0}_{3\times3}\\ \mathbf{0}_{3\times3} & \mathbf{0}_{3\times3}\end{bmatrix},\ \mathbf{I}_\gamma = \begin{bmatrix}\mathbf{I}_{3\times3}\\ \mathbf{0}_{3\times3}\end{bmatrix}^T.$$

The superscript "$-$" indicates that corresponding variables are estimates before corrections. The rotation matrix ${}^G_{k+1}\boldsymbol{\mathcal{R}}$ denotes the orientation relationship between the NED coordinate and the vehicle fixed coordinate at time $k+1$.

2) Full-state model: Since this work focuses on the localization of DAUVs, for each DAUV, orientations of MAUVs and other DAUVs in the sensor range do not provide useful localization information. Even though the relative orientation relation among AUVs is important in cooperative measurements fusion, such topics are out of the scope of this work. Thus, the full-state vector for DAUV 1 is $\boldsymbol{\mu} = \begin{bmatrix}\mathbf{x}_{D_1}^T & \mathbf{p}_{D_2}^T & \cdots & \mathbf{p}_{D_d}^T & \mathbf{p}_{M_1}^T & \mathbf{p}_{M_2}^T & \cdots & \mathbf{p}_{M_m}^T\end{bmatrix}^T$, of which the dimension is $L \times 1$ and $L = 6 + 3(d-1) + 3m$. Since motion models and paths of other AUVs are not known by DAUV 1, they submit their position estimates when entering the communication range of DAUV 1. Therefore, the total control input is also a $L \times 1$ vector in the form of $\mathbf{u} = [\boldsymbol{\tau}_{D_1}^T \quad \mathbf{p}_{D_2}^T \quad \cdots \quad \mathbf{p}_{D_d}^T \quad \mathbf{p}_{M_1}^T \quad \mathbf{p}_{M_2}^T \quad \cdots \quad \mathbf{p}_{M_m}^T]^T$. $\mathbf{p}_{D_i}\ (i = 2, 3, \cdots, d)$ and $\mathbf{p}_{M_j}\ (j = 1, 2, \cdots, m)$ are position estimates of the other DAUVs and MAUVs respectively, updated when they enter the sensor range or kept as old values otherwise. This is reasonable since we only concern the position of DAUV 1, and positions of other AUVs are trivial unless they are used in the estimate correction. Then the full-state motion model is

$$\boldsymbol{\mu}^-_{k+1} = \mathbf{f}\left(\ \boldsymbol{\mu}_k, \mathbf{u}_{k+1}, \boldsymbol{\omega}_{k+1}\ \right), \tag{5}$$

where $\boldsymbol{\omega}$ are control noises with mean $\mathbf{0}$ and covariance $\mathbf{Q}$.

B. EKF prediction

The EKF linearizes the nonlinear motion model using Taylor series expansion. The motion prediction is based on the noise-free full-state time updating method, which is

$$\begin{aligned}\boldsymbol{\mu}^-_{k+1} &= \mathbf{f}\left(\ \boldsymbol{\mu}_k, \mathbf{u}_{k+1}, \mathbf{0}\ \right)\\ &= \mathcal{I}_L^T\left(\ \mathcal{I}_L\boldsymbol{\mu}_k + {}^G_{k+1}\mathcal{R}\ \mathcal{I}_L\mathbf{u}_{k+1}\delta t\ \right) + \mathcal{I}_C\mathbf{u}_{k+1}.\end{aligned} \tag{6}$$

$$\mathcal{I}_L = \left[\mathbf{I}_{3\times3} \quad \mathbf{0}_{3\times(L-3)}\right],$$

$$\mathcal{I}_C = \begin{bmatrix}\mathbf{0}_{3\times3} & \mathbf{0}_{3\times3} & \mathbf{0}_{3\times(L-6)}\\ \mathbf{0}_{3\times3} & \mathbf{I}_{3\times3} & \mathbf{0}_{3\times(L-6)}\\ \mathbf{0}_{(L-6)\times3} & \mathbf{0}_{(L-6)\times3} & \mathbf{0}_{(L-6)\times(L-6)}\end{bmatrix}.$$

Equation (6) is the motion propagation of DAUV 1. The first term translates the DAUV 1 to a new position based on the control input. The second term updates the orientation based on the latest Euler angle measurement. This motion updating process repeats at each time step, during which the covariance matrix $\boldsymbol{\Sigma}$ also updates based on

$$\boldsymbol{\Sigma}^-_{k+1} = \mathbf{F}_{\boldsymbol{\mu}}\boldsymbol{\Sigma}_k\mathbf{F}^T_{\boldsymbol{\mu}} + \mathbf{F}_{\boldsymbol{\omega}}\mathbf{Q}_{k+1}\mathbf{F}^T_{\boldsymbol{\omega}}, \tag{7}$$

where $\mathbf{F}_{\boldsymbol{\mu}}$ and $\mathbf{F}_{\boldsymbol{\omega}}$ are Jacobian matrices.

C. Observation model

Assume DAUV 1 takes range and bearing measurements of neighbor DAUVs and MAUVs every a fixed number of time steps. Among all vehicles, MAUVs carry more accurate localization information. DAUVs first search for available MAUVs in the sensor range to take measurements and perform positioning corrections. Each measurement is a 3×1 vector in spherical coordinates $\begin{bmatrix}r_n & \alpha_n & \beta_n\end{bmatrix}^T$ in the form

$$\mathbf{z}_n = \begin{bmatrix}s & \arccos\left(\delta z_{nD_1}/s\right) & \text{atan2}\left(\delta y_{nD_1}/\delta x_{nD_1}\right)\end{bmatrix}^T \tag{8}$$

for $\{\ n \mid n \in \{D_2, \cdots, D_d, M_1, \cdots, M_m\}\ \cap\ r_n \le S\ \}$, where $s = \sqrt{{\delta x_{nD_1}}^2 + {\delta y_{nD_1}}^2 + {\delta z_{nD_1}}^2}$, S is the range of the sensor and $\delta x_{nD_1} = x_n - x_{D_1}$. Hence the measurement model can be written as

$$\begin{aligned}\tilde{\mathbf{z}}_{k+1} &= \mathbf{h}\left(\boldsymbol{\mu}^-_{k+1}, \boldsymbol{\nu}_{k+1}\right)\\ &= \begin{bmatrix}\mathbf{z}_{2,k+1}^T & \mathbf{z}_{3,k+1}^T & \cdots & \mathbf{z}_{d+m,k+1}^T\end{bmatrix}^T + \boldsymbol{\nu}_{k+1},\end{aligned} \tag{9}$$

where $\boldsymbol{\nu}$ are measurement noises with mean $\mathbf{0}$ and covariance $\mathbf{R}$.

D. Intra-AUV data fusion

The correlation among AUVs is the key to the algorithm. Roumeliotis and Bekey [12] investigated the propagation of covariance matrices in robot group in centralized form and discussed how this problem can be decomposed into a distributed form. The computation is distributed among multiple robots while the whole estimated state vector and covariance matrix are still stored in a centralized manner. Our algorithm, on the other hand, is fully distributed. Each DAUV has a unique state vector and covariance matrix. In general, in the three-vehicle case, the covariance matrix used by Vehicle 1 can be described as

$$\boldsymbol{\Sigma} = \begin{bmatrix}\boldsymbol{\Sigma}_{11} & \boldsymbol{\Sigma}_{12} & \boldsymbol{\Sigma}_{13}\\ \boldsymbol{\Sigma}_{21} & \boldsymbol{\Sigma}_{22} & \mathbf{0}\\ \boldsymbol{\Sigma}_{31} & \mathbf{0} & \boldsymbol{\Sigma}_{33}\end{bmatrix}.$$

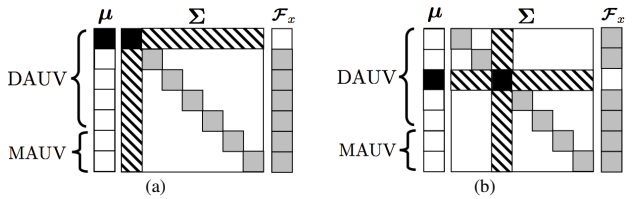

Fig. 3. Data structure in the 5 DAUVs and 2 MAUVs case. (a) shows the information stored in DAUV 1. Black squares stand for the state or the variance of DAUV 1. Grey squares in the covariance matrix stand for variances of other AUVs. Grey squares in the Jacobian multiplier stand for accumulated multipliers for the corresponding vehicles since the last meet. Dashed squares stand for the cross-correlation between DAUV 1 and other AUVs. Similarly, (b) shows information stored by DAUV 3.

Due to the distributed feature, the motion update of Vehicle 1 can affect the covariance matrix to the degree of

$$\boldsymbol{\Sigma} = \begin{bmatrix} \mathbf{F}_{\mathbf{x}_1}\boldsymbol{\Sigma}_{11}\mathbf{F}_{\mathbf{x}_1}^T + \mathbf{F}_{\boldsymbol{\omega}}\mathbf{Q}\mathbf{F}_{\boldsymbol{\omega}}^T & \mathbf{F}_{\mathbf{x}_1}\boldsymbol{\Sigma}_{12} & \mathbf{F}_{\mathbf{x}_1}\boldsymbol{\Sigma}_{13} \\ \boldsymbol{\Sigma}_{21}\mathbf{F}_{\mathbf{x}_1}^T & \boldsymbol{\Sigma}_{22} & \mathbf{0} \\ \boldsymbol{\Sigma}_{31}\mathbf{F}_{\mathbf{x}_1}^T & \mathbf{0} & \boldsymbol{\Sigma}_{33} \end{bmatrix}.$$

After l steps of movements without information exchange with other vehicles, cross-correlation terms in the covariance matrix turn into $\boldsymbol{\Sigma}_{1j}^{k+l} = \mathbf{F}_{x_1}^{k+l}\cdots\mathbf{F}_{x_1}^{k+2}\mathbf{F}_{x_1}^{k+1}\boldsymbol{\Sigma}_{1j}^{k}$, $(j = 2, 3)$. But these cross-correlation terms need to be multiplied by $\boldsymbol{\mathcal{F}}_{ji} = \mathbf{F}_{x_j}^{k+l}\mathbf{F}_{x_j}^{k+l-1}\cdots\mathbf{F}_{x_j}^{k+2}\mathbf{F}_{x_j}^{k+1}$ or $\boldsymbol{\mathcal{F}}_{ji}^T$, denoted as the Jacobian multiplier stored in vehicle j for vehicle i, to complete the prediction. These multipliers are also used in the motion updates of the covariance matrices of Vehicle 2 and Vehicle 3 respectively. As a result, information needed from other vehicles are their own variances $\boldsymbol{\Sigma}_{jj}$ and accumulated Jacobian multipliers $\boldsymbol{\mathcal{F}}_{j1}$ since their last meet with Vehicle 1. Cross-correlation terms among all other vehicles except for j are set to zeros. This is crucial since for Vehicle 1, the Kalman gain used to update its own position estimates includes all terms of the covariance matrix. Terms related to other vehicles out of the sensor range are not updated and hence are not correct. The new covariance matrix after fusing information from Vehicle 3, for example, will be

$$\hat{\boldsymbol{\Sigma}} = \begin{bmatrix} \underline{\boldsymbol{\mathcal{F}}_{11}\boldsymbol{\Sigma}_{11}\boldsymbol{\mathcal{F}}_{11}^T + \boldsymbol{\mathcal{F}}_{\boldsymbol{\omega}}\mathbf{Q}\boldsymbol{\mathcal{F}}_{\boldsymbol{\omega}}^T} & \boldsymbol{\mathcal{F}}_{11}\boldsymbol{\Sigma}_{12} & \underline{\boldsymbol{\mathcal{F}}_{11}\boldsymbol{\Sigma}_{13}\boldsymbol{\mathcal{F}}_{31}^T} \\ \boldsymbol{\Sigma}_{21}\boldsymbol{\mathcal{F}}_{11}^T & \boldsymbol{\Sigma}_{22} & \mathbf{0} \\ \underline{\boldsymbol{\mathcal{F}}_{31}\boldsymbol{\Sigma}_{31}\boldsymbol{\mathcal{F}}_{11}^T} & \mathbf{0} & \underline{\boldsymbol{\Sigma}_{33}} \end{bmatrix},$$

where all underlined terms are updated and can be used in the correction step. Fig. 3 shows structures in which this information is stored in particular DAUVs.

a) DAUV-MAUV Data Fusion: Even though MAUVs have errors in their position estimates using DR and MLBL, better on-board equipment and intermittent accesses to global positioning references through MLBL guarantee that they possess much more accurate localization information than all DAUVs. When DAUVs take measurements, they first search for MAUVs for localization corrections. There may be more than one MAUV in the sensor range, all of which will be used in such a case. MAUVs' position estimates used in the DAUV's measurement model are submitted by corresponding MAUVs, along with their variance $\boldsymbol{\Sigma}_{jj}$ $(j = 1, 2, \ldots m)$ and the accumulated Jacobian multiplier $\boldsymbol{\mathcal{F}}_{ji}$. At the same time, acquired marine date can also be transferred to MAUVs. After performing corrections with any MAUVs, further "corrections" with any other neighbor DAUVs at the same time step will result in no better state estimates. However, the intra-DAUV correction will contribute a lot to some DAUVs when MAUVs are not detected, especially for a very long time.

b) Intra-DAUV Data Fusion: The intra-DAUV data fusion takes place when two DAUVs enter into the sensor range of each other, which needs to be carefully accounted for because of the distributed feature. It is known that the measurement being used by a particular AUV for more than once leads to inconsistent or overconfident estimates [18]. We use one-way data fusion to avoid measurement reusing. In addition, each DAUV performs relative measurements and communications with only one neighbor DAUV in the sensor range during its measurement stage. When there are more than one neighbor DAUV in the sensor range, a proper selection technique is necessary to ensure that the DAUVs get the best localization correction in intra-DAUV data fusion. Since the absolute localization error is not known, one reasonable alternative is the variance of the position estimates, which stands for the degree of spreading out of the estimates distribution. For example, in the three-dimensional case, we take the trace of the variance of DAUV n, *i.e.* trace($\boldsymbol{\Sigma}_{nn}$), evaluated by DAUV n itself.

E. EKF correction

Since only vehicles in the sensor range can provide potential localization correction information for vehicles out of the sensor range, the full-state vector still keeps their old location information submitted when they were detected earlier. But actual measurement data are all zeros. For these vehicles, naively applying the correction equation will introduce large modeling errors. This can be fixed by introducing a selection matrix $\boldsymbol{\Xi}$ with submatrices

$$\boldsymbol{\xi}_i = \begin{cases} \mathbf{I}_{3\times3} & \text{for} \quad n = D_i \cup \{n \neq D_i \mid r_n \leq S\}; \\ \mathbf{0}_{3\times3} & \text{for} \quad \{n \neq D_i \mid r_n > S\}. \end{cases},$$

where $n \in \{D_1, \cdots, D_d, M_1, \cdots, M_m\}$ such that $\boldsymbol{\Xi}$ is a diagonal matrix with $\boldsymbol{\xi}_{D_1}, \boldsymbol{\xi}_{D_2}, \cdots, \boldsymbol{\xi}_{M_m}$ as diagonal submatrices and 0 anywhere else. Define $\hat{\boldsymbol{\Sigma}}_{k+1}^{*-} = \boldsymbol{\Xi}\,\hat{\boldsymbol{\Sigma}}_{k+1}^{-}\,\boldsymbol{\Xi}^T$ as the covariance matrix only with fully updated terms and zeros anywhere else, then the EKF correction is based on

$$\boldsymbol{\mu}_{k+1} = \boldsymbol{\mu}_{k+1}^{-} + \mathbf{K}_{k+1}\left[\tilde{\mathbf{z}}_{k+1} - \mathbf{h}\left(\boldsymbol{\mu}, \mathbf{0}\right)\right], \tag{10}$$

where $\mathbf{K}_{k+1}$ is the Kalman gain, which has the form

$$\mathbf{K}_{k+1} = \hat{\boldsymbol{\Sigma}}_{k+1}^{*-}\mathbf{H}_{\boldsymbol{\mu}}^T\left(\mathbf{H}_{\boldsymbol{\mu}}\hat{\boldsymbol{\Sigma}}_{k+1}^{*-}\mathbf{H}_{\boldsymbol{\mu}}^T + \mathbf{R}_{k+1}\right)^{-1}, \tag{11}$$

and the covariance matrix correction will be

$$\hat{\boldsymbol{\Sigma}}_{k+1} = \hat{\boldsymbol{\Sigma}}_{k+1}^{-} - \mathbf{K}_{k+1}\mathbf{H}_{\boldsymbol{\mu}}\hat{\boldsymbol{\Sigma}}_{k+1}^{*-}. \tag{12}$$

Selection matrices filter out terms with dated data in covariance matrices to make sure the correctness of the updating process. In the three vehicles case, when Vehicle 3 is observed by Vehicle 1, the covariance matrix before being

updated and the selection matrix stored by Vehicle 1 are

$$\boldsymbol{\Sigma}^{-}_{k+1} = \begin{bmatrix} \boldsymbol{\Sigma}_{11} & \boldsymbol{\Sigma}_{12} & \boldsymbol{\Sigma}_{13} \\ \boldsymbol{\Sigma}_{21} & \boldsymbol{\Sigma}_{22} & \mathbf{0} \\ \boldsymbol{\Sigma}_{31} & \mathbf{0} & \boldsymbol{\Sigma}_{33} \end{bmatrix} \text{ and } \boldsymbol{\Xi}_{k+1} = \begin{bmatrix} \mathbf{I}_3 & \mathbf{0}_3 & \mathbf{0}_3 \\ \mathbf{0}_3 & \mathbf{0}_3 & \mathbf{0}_3 \\ \mathbf{0}_3 & \mathbf{0}_3 & \mathbf{I}_3 \end{bmatrix}.$$

$$\boldsymbol{\Sigma}^{*-}_{k+1} = \boldsymbol{\Xi}_{k+1}\,\boldsymbol{\Sigma}^{-}_{k+1}\,\boldsymbol{\Xi}^{T}_{k+1} = \begin{bmatrix} \boldsymbol{\Sigma}_{11} & \mathbf{0}_3 & \boldsymbol{\Sigma}_{13} \\ \mathbf{0}_3 & \mathbf{0}_3 & \mathbf{0}_3 \\ \boldsymbol{\Sigma}_{31} & \mathbf{0}_3 & \boldsymbol{\Sigma}_{33} \end{bmatrix}. \quad (13)$$

If we use a Cartesian measurement model, $\mathbf{h} = \begin{bmatrix} dx & dy & dz \end{bmatrix}^T$, to simplify the form of $\mathbf{H}_{\boldsymbol{\mu}}$ for a better explanation, the innovation covariance can be computed as

$$\begin{aligned} \mathbf{S}_{k+1} &= \mathbf{H}_{\boldsymbol{\mu}} \boldsymbol{\Sigma}^{*-}_{k+1} \mathbf{H}^{T}_{\boldsymbol{\mu}} + \mathbf{R}_{k+1} \\ &= \boldsymbol{\Sigma}_{11} - \boldsymbol{\Sigma}_{13} - \boldsymbol{\Sigma}_{31} + \boldsymbol{\Sigma}_{33} + \mathbf{R}_{k+1}, \end{aligned} \quad (14)$$

where $\mathbf{H}_{\boldsymbol{\mu}} = \begin{bmatrix} -\mathbf{I}_3 & \mathbf{0}_3 & \mathbf{I}_3 \end{bmatrix}$ and all terms are updated correctly. The second term in (12) can be calculated as

$$\mathbf{K}_{k+1}\mathbf{H}_{\boldsymbol{\mu}}\boldsymbol{\Sigma}^{*-}_{k+1} = \begin{bmatrix} \boldsymbol{\mathcal{X}}_{11} & \mathbf{0}_3 & \boldsymbol{\mathcal{X}}_{13} \\ \mathbf{0}_3 & \mathbf{0}_3 & \mathbf{0}_3 \\ \boldsymbol{\mathcal{X}}_{31} & \mathbf{0}_3 & \boldsymbol{\mathcal{X}}_{33} \end{bmatrix}, \quad (15)$$

where all $\boldsymbol{\mathcal{X}}$ terms only include $\boldsymbol{\Sigma}_{11}$, $\boldsymbol{\Sigma}_{13}$, $\boldsymbol{\Sigma}_{31}$, $\boldsymbol{\Sigma}_{33}$, and $\mathbf{R}_{k+1}$. The correction just affects corresponding terms in $\boldsymbol{\Sigma}^{-}_{k+1}$ and only correctly updated terms are used. When there are p MAUVs in the sensor range of DAUV i, it updates corresponding terms and correct estimates based on Algorithm 1. When there are no MAUVs but neighbor DAUVs in the sensor range, DAUV i updates corresponding terms and correct estimates according to information from the DAUV with the smallest variance trace.

Algorithm 1 DAUV-MAUV Data Fusion

1: **for** j = 1 to p **do**
2: $\quad \boldsymbol{\mu}^{-}_{i,k+1} \leftarrow \{\boldsymbol{\mu}^{-}_{i,k+1}, \boldsymbol{\mu}_{j,k+1}\}$
3: $\quad \hat{\boldsymbol{\Sigma}}^{-}_{i,k+1} \leftarrow \{\boldsymbol{\Sigma}^{-}_{i,k+1}, \boldsymbol{\Sigma}_{jj,k+1}, \boldsymbol{\mathcal{F}}_{j,k+1}\}$
4: $\quad$ Reset $\boldsymbol{\mathcal{F}}_{ij,k+1}$
5: $\quad \mathbf{K}_{i,k+1} \leftarrow \{\hat{\boldsymbol{\Sigma}}^{-}_{i,k+1}, \mathbf{H}_{\boldsymbol{\mu},i}, \mathbf{R}_{i,k+1}, \boldsymbol{\Xi}_{i,k+1}\}$
6: $\quad \boldsymbol{\mu}_{i,k+1} \leftarrow \{\boldsymbol{\mu}^{-}_{i,k+1}, \mathbf{K}_{i,k+1}, \tilde{\mathbf{z}}_{i,k+1}, \mathbf{z}_{i,k+1}\}$
7: $\quad \boldsymbol{\Sigma}_{i,k+1} \leftarrow \{\hat{\boldsymbol{\Sigma}}^{-}_{i,k+1}, \mathbf{H}_{\boldsymbol{\mu},i}, \mathbf{K}_{i,k+1}, \boldsymbol{\Xi}_{i,k+1}\}$
8: **end for**

IV. Simulations and Results

We consider an extended double-gyre flow type in 3-dimensional space by wrapping four convection cells around a cylinder. The resulting finite-time Lyapunov exponent (FTLE) and LCS are generalized by Lekien and Ross in [19]. Fig. 4 shows simulated paths of one MAUV and three DAUVs. The performance comparison between using pure DR and the proposed algorithm is shown in Fig. 5. Deviations of estimated paths from real paths are bounded because of localization information provided by the MAUV. The improvement will be more obvious as the run-time increases. The effect of the number of MAUVs is examined in Fig. 6. Improvements on upper bounds are noticed. Average errors decrease since DAUVs have more chances to perform localization corrections with MAUVs. When a particular DAUV finishes the correction with at least one MAUV, it acts

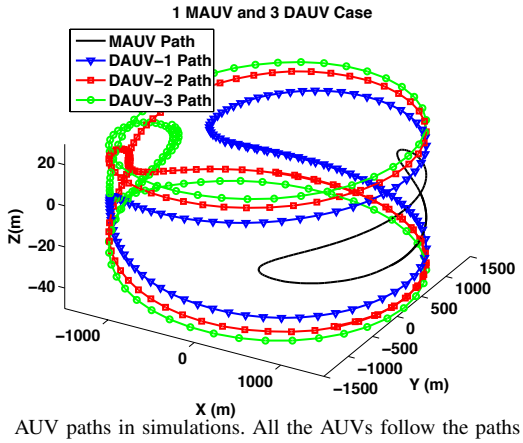

Fig. 4. AUV paths in simulations. All the AUVs follow the paths created based on the FTLE on the cylinder.

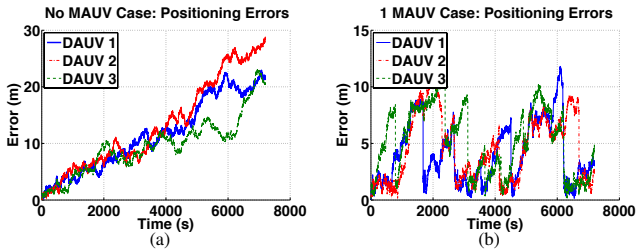

Fig. 5. Positioning errors of three DAUVs when (a) only using DR and (b) performing the proposed algorithm with 1 MAUV.

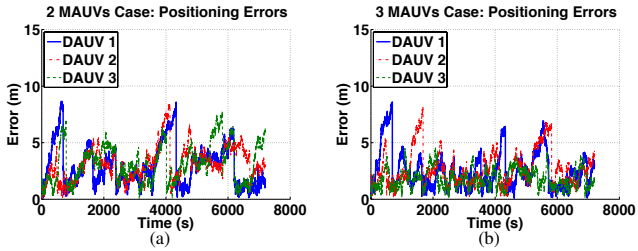

Fig. 6. Positioning errors of three DAUVs when performing the proposed algorithm with (a) 2 MAUVs and (b) 3 MAUVs.

as a virtual MAUV for a short time due to its small variance after the correction. The upper bound is affected by DR errors of MAUVs, actual paths of AUVs under the influence of background flow and the noise level of intra-vehicle measurements. It can also be concluded that a good MAUV path planning method adapted to the flow will increase the occurrence rate of DAUV-MAUV measurements and data fusion, and hence improve the localization of DAUVs, which is one of our further research focuses.

A more common flow pattern, the flow generated by vortices on a sphere, is widely used in geophysical fluid dynamics when considering large-scale atmospheric or oceanographic flow with coherent structures that persist over a long period of time and move over large distances. This flow pattern is used as a simplified model of global ocean currents by ignoring interactions with lands. Ocean vortices are simulated by moving point vortices and the resulting flow pattern can be used in meteorology study including hurricane simulations. We focus on a special solution discussed by Kidambi and Newton in [20]. Three vortices move under the impact of the others (Fig. 7) and the vortices paths can be expressed in the Cartesian coordinate as

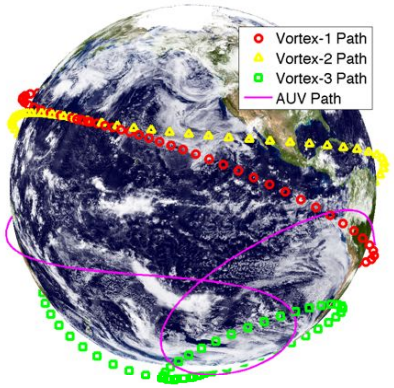

Fig. 7. Non-dimensional vehicle path driven by the background flow generated by three vortices on a unit sphere.

TABLE I

80% UPPER BOUNDS OF THE AVERAGE LOCATION ERROR

Number of MAUVs	Error of MAUVs (m)	3 DAUVs	5 DAUVs	10 DAUVs
1	[-1,1]	7.48m	7.30m	7.37m
3	[-1,1]	4.82m	4.37m	4.19m
3	[-3,3]	7.80m	7.21m	6.42m

$$\dot{\mathbf{x}}_i = \frac{1}{4\pi R} \sum_{j \neq i}^{N} \Gamma_j \frac{\mathbf{x}_j \times \mathbf{x}_i}{R^2 - \mathbf{x}_i \cdot \mathbf{x}_j}, \tag{16}$$

where $\mathbf{x}_i$ is the location of vortex i, Γ_j is the vorticity of vortex j located at $\mathbf{x}_j$, N is the total number of vortices and R is the radius of the sphere [21]. In each simulation, we evaluate the 80% upper bounds of average location errors among all DAUVs, under which the average location error lies for 80% of the run-time. Table I shows results of these simulations. For a given number of MAUVs, increasing the number of DAUVs slightly decreases bounds. This is because a larger number of DAUVs increase the propagation rate of localization information from MAUVs. While, the decrease in the 80% upper bounds caused by increasing the number of MAUVs is dramatic. Since more references are available, DAUVs have a bigger change to meet MAUVs. When localization errors of MAUVs increase, upper bounds also rise. Due to the randomness of Gaussian noises in different simulations, the increase is not strictly linear.

V. CONCLUSIONS

We use several mother AUVs with bounded localization errors as moving references to improve localization of low-cost daughter AUVs based on recent progresses on optimized path planning in strong background flow fields. Daughter AUVs take relative measurements and exchange information to slow down increases of DR errors and to propagate localization correction information from mother AUVs. The proposed algorithm is fully distributed, making it practical in large-scale applications. The correlation among AUVs is properly accounted for. Simulation results are consistent with the theory. The accuracy of MLBL, the stability of range and bearing sensors, the Gaussian noise assumption and linearization errors using EKF require further investigations. Further work will also focus on the robustness of the algorithm and we believe that background flow can also provide localization information if properly considered. Experiments will be done to prove the thoery and to identify limitations.

REFERENCES

[1] H.-P. Tan, R. Diamant, W. K. Seah, and M. Waldmeyer, "A survey of techniques and challenges in underwater localization," *Ocean Engineering*, vol. 38, no. 14 - 15, pp. 1663 – 1676, 2011.

[2] J. Aulinas, Y. R. Petillot, X. Llad, J. Salvi, and R. Garcia, "Vision-based underwater SLAM for the SPARUSAUV," in *Proceedings of the 10th International Conference on Computer and IT Applications in the Maritime Industries (COMPIT)*, Berlin, Germany, May 2011, pp. 171–181.

[3] A. Bahr, J. J. Leonard, and M. F. Fallon, "Cooperative localization for autonomous underwater vehicles," *The International Journal of Robotics Research*, vol. 28, no. 6, pp. 714–728, 2009.

[4] Y. Zhou, K. Chen, J. He, J. Chen, and A. Liang, "A hierarchical localization scheme for large scale underwater wireless sensor networks," in *High Performance Computing and Communications, 2009. HPCC '09. 11th IEEE International Conference on*, June, pp. 470–475.

[5] D. Lipinski and K. Mohseni, "A ridge tracking algorithm and error estimate for efficient computation of Lagrangian coherent structures," *Chaos*, vol. 20, p. 017504 (9pp.), 2010, doi:10.1063/1.3270049.

[6] T. Inanc, S. Shadden, and J. Marsden, "Optimal trajectory generation in ocean flows," in *American Control Conference, 2005. Proceedings of the 2005*, 2005, pp. 674–679.

[7] D. Lipinski and K. Mohseni, "Cooperative control of a team of unmanned vehicles using smoothed particle hydrodynamics," AIAA Guidance, Navigation, and Control Conference, Toronto, Ontario, Canada, Tech. Rep., August 2010.

[8] ——, "A master-slave fluid cooperative control algorithm for optimal trajectory planning," in *IEEE International Conference on Robotics and Automation*, Shanghai, China, 9-13 May 2011, paper WeA212.2.

[9] J. Vaganay, J. Leonard, J. Curcio, and J. Willcox, "Experimental validation of the moving long base-line navigation concept," in *Autonomous Underwater Vehicles, 2004 IEEE/OES*, june 2004, pp. 59–65.

[10] J. Curcio, J. Leonard, J. Vaganay, A. Patrikalakis, A. Bahr, D. Battle, H. Schmidt, and M. Grund, "Experiments in moving baseline navigation using autonomous surface craft," in *OCEANS, 2005. Proceedings of MTS/IEEE*, vol. 1, 2005, pp. 730–735.

[11] A. Martinelli, F. Pont, and R. Siegwart, "Multi-robot localization using relative observations," in *IEEE International Conference on Robotics and Automation (ICRA)*, April 2005, pp. 2797–2802.

[12] S. I. Roumeliotis and G. A. Bekey, "Distributed multirobot localization," *IEEE Transactions on Robotics and Automation*, vol. 18, pp. 781–795, 2002.

[13] K. Mohseni, "Pulsatile vortex generators for low-speed maneuvering of small underwater vehicles," *Ocean Engineering*, vol. 33, no. 16, pp. 2209–2223, 2006.

[14] M. Krieg and K. Mohseni, "Thrust characterization of pulsatile vortex ring generators for locomotion of underwater robots," *IEEE J. Oceanic Engineering*, vol. 33, no. 2, pp. 123–132, 2008.

[15] ——, "Dynamic modeling and control of biologically inspired vortex ring thrusters for underwater robot locomotion," *IEEE Trans. Robotics*, vol. 26, no. 3, pp. 542–554, 2010.

[16] M. Krieg, P. Klein, R. Hodgkinson, and K. Mohseni, "A hybrid class underwater vehicle: bioinspired propulsion, embedded system, and acoustic communication and localization system," *Marine Technology Society Journal: Special Edition on Biomimetics and Marine Technology*, vol. 45, no. 4, pp. 153–164, 2011.

[17] C.-C. Wang, C. Thorpe, and S. Thrun, "Online simultaneous localization and mapping with detection and tracking of moving objects: Theory and results from a ground vehicle in crowded urban areas," in *IEEE International Conference on Robotics and Automation (ICRA)*, 2003, pp. 842–849.

[18] A. Bahr, M. Walter, and J. Leonard, "Consistent cooperative localization," in *Robotics and Automation, 2009. ICRA '09. IEEE International Conference on*, 2009, pp. 3415–3422.

[19] F. Lekien and S. Ross, "The computation of finite-time Lyapunov exponents on unstructured meshes and for non-Euclidean manifolds," *Chaos*, vol. 20, p. 017504, 2010.

[20] R. Kidambi and P. K. Newton, "Motion of three point vortices on a sphere," *Physica D: Nonlinear Phenomena*, vol. 116, pp. 143–175, 1998.

[21] P. Newton, *The N-Vortex Problem: Analytical Techniques*, ser. Applied Mathematical Sciences. Springer, 2001, no. v. 145.